NASA/TM—1998-208653

AIAA–98–4863

The Role of Multiphysics Simulation in Multidisciplinary Analysis

Steven M. Rifai, Robert M. Ferencz, Wen-Ping Wang,
and Evangelos T. Spyropoulos
Centric Engineering Systems, Inc., Sunnyvale, California

Charles Lawrence and Matthew E. Melis
Lewis Research Center, Cleveland, Ohio

Prepared for the
Symposium on Multidisciplinary Analysis and Optimization
sponsored by the American Institute of Aeronautics and Astronautics
St. Louis, Missouri, September 2–4, 1998

National Aeronautics and
Space Administration

Lewis Research Center

October 1998

Acknowledgments

Portions of this work were supported under the NASA High Performance Computing and Communication Program (HPCCP). Centric gratefully acknowledges this support as well as that provided by our commercial customers.

Available from

NASA Center for Aerospace Information
7121 Standard Drive
Hanover, MD 21076
Price Code: A03

National Technical Information Service
5285 Port Royal Road
Springfield, VA 22100
Price Code: A03

THE ROLE OF MULTIPHYSICS SIMULATION IN MULTIDISCIPLINARY ANALYSIS

Steven M. Rifai, Robert M. Ferencz, Wen-Ping Wang, Evangelos T. Spyropoulos
Centric Engineering Systems, Inc., Sunnyvale, CA 94086

Charles Lawrence, Matthew E. Melis
NASA Lewis Research Center, Cleveland, Ohio 44135

Abstract

This article describes the application of the Spectrum™ Solver in Multidisciplinary Analysis (MDA). Spectrum, a multiphysics simulation software based on the finite element method, addresses compressible and incompressible fluid flow, structural, and thermal modeling as well as the interaction between these disciplines. Multiphysics simulation is based on a single computational framework for the modeling of multiple interacting physical phenomena. Interaction constraints are enforced in a fully-coupled manner using the augmented-Lagrangian method. Within the multiphysics framework, the finite element treatment of fluids is based on the Galerkin-Least-Squares (GLS) method with discontinuity capturing operators. The arbitrary-Lagrangian-Eulerian method is utilized to account for deformable fluid domains. The finite element treatment of solids and structures is based on the Hu-Washizu variational principle. The multiphysics architecture lends itself naturally to high-performance parallel computing. Aeroelastic, propulsion, thermal management and manufacturing applications are presented.

1. Introduction

Many of the current directions in product design and analysis are driven by competitive and regulatory constraints, such as the need to shorten design cycles, reduce cost, meet increasingly stringent government regulations, improve quality and safety, and reduce environmental impact. These directions have increased the need for accurate product and component simulation and pressed analysts for simulations of unprecedented scale and complexity. For example, aeroelastic modeling (figure 1), involving strong coupling of fluids and structures, is an essential element in the design process of aircraft. Thermal management issues arising from automotive, aeropropulsion and aerospace design and manufacturing applications require the coupled analysis of fluids, thermal and structural models. In general, flow-induced vibrations are a primary concern in the aerospace, automotive and defense industries.

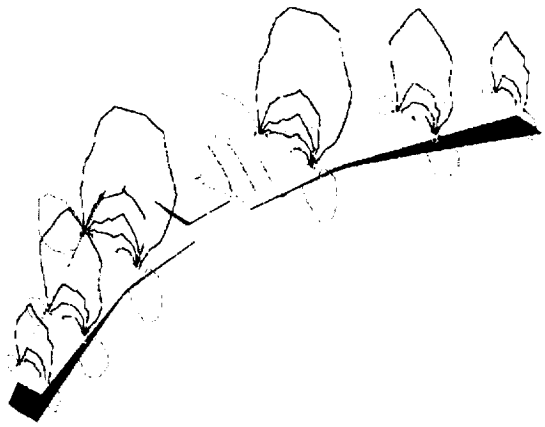

Figure 1. Aeroelastic simulation of the ARW2 wing configuration.

The high-fidelity simulation of multidisciplinary interactions is computationally expensive. While single processor computers improve every year, the quantum increase in computational needs requires a quantum increase in computational power. The hardware industry has answered this increased need with affordable high-performance parallel architectures which are built on commodity parts and compatible with workstation systems. The multiphysics architecture used in this work lends itself naturally to high-performance parallel computing. Coarse grain parallel processing is utilized through the SPMD paradigm with domain decomposition. Within each problem subdomain, super-scalar, vector processing and cache efficiency is leveraged with element blocking schemes.

2. The Multiphysics Problem Model

The multiphysics architecture supports multiple physical interactions through a data model defined as a hierarchical tree of regions and interfaces[1]. Regions of a problem are used to separate the different physics being analyzed over the spatial domain. For example, in a fluid-structure interaction (FSI) problem, the fluid

domain is one region and the solid structure is another (figure 2). Interfaces are used to enforce the coupling constraints between the different regions.

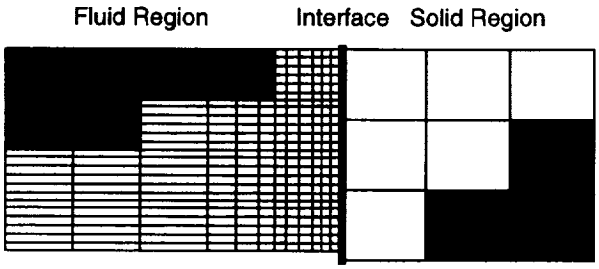

Figure 2. Multiphysics problem domain.

Because of the varying discretization requirements of the different physical phenomena, this approach is designed to allow variable mesh densities and element topologies at the region interfaces. The finite element formulation admits (automatically generated) unstructured meshes. For example, in a typical FSI problem, a highly refined tetrahedral mesh may be used to model the fluid domain with a relatively coarse hexahedral discretization representing the solid region. These discretizations do not, in general, coincide at the shared region boundaries.

3. Fluid Regions

The finite element treatment of fluid regions within this framework is based on the Galerkin-Least-Squares (GLS) method with discontinuity capturing operators[3-5]. Reynolds-averaged and Large-Eddy-Simulation models are utilized for turbulence simulation[6]. In this treatment, the compressible flow formulation makes use of *physical entropy variables*, $\boldsymbol{V}$. With these variables, the fluid conservation laws are expressed in symmetric form which intrinsically expresses the mathematical and physical stability provided by the second law of thermodynamics. Specifically, the Navier-Stokes equation system is expressed in the form

$$\tilde{\boldsymbol{A}}_0 \boldsymbol{V}_{,t} + \tilde{\boldsymbol{A}}_i \boldsymbol{V}_{,i} = (\tilde{\boldsymbol{K}}_{ij} \boldsymbol{V}_{,j})_{,i} + \tilde{\boldsymbol{F}}^{src} \tag{1}$$

In turn, the finite element techniques employed herein inherit this fundamental stability and convergence proofs are available[7].

Multiphysics problems often require the movement of the computational fluid domain in response to the deformation of the common solid region boundaries. The arbitrary-Lagrangian-Eulerian (ALE) method is utilized to account for the deformations in fluid domains[8].

ALE boundary conditions ensure that the deforming mesh conforms to both the stationary and moving boundaries. Within the interior of the fluid domain, mesh movement is modeled by the equations of large deformation elasticity. In effect, this model computes the position of the interior nodes as if all nearest nodal neighbors were coupled by an elastic medium and sets the positions and velocities of the boundary nodes to exactly match the boundary motions. Note that this model is a purely mathematical construct; it is a method for updating the mesh in a way that has a reasonable chance of maintaining mesh integrity. Thus, terms such as Cauchy stresses, elastic moduli, and so forth do not have the usual physical interpretation within this context.

To take mesh movement into account, the convective or Euler flux in equation (1) is replaced by the ALE convective flux. The ALE convective flux is related to the Euler flux by the equation

$$\boldsymbol{F}_i^{ALE} = \boldsymbol{F}_i^{conv} - u_i^{ALE} \boldsymbol{U} \tag{2}$$

where $\boldsymbol{u}^{ALE}$ is the velocity field of the mesh. The Euler Jacobians of equation (1) become

$$\tilde{\boldsymbol{A}}_i^{ALE} = \tilde{\boldsymbol{A}}_i - u_i^{ALE} \tilde{\boldsymbol{A}}_0 \,. \tag{3}$$

4. Solid Regions

The finite element treatment of solid regions within this framework employs a 3-field formulation based on the Hu-Washizu variational principle. This method is well documented in the literature to address numerical locking phenomena[10]. The kinematic description admits small and finite deformations and strains. Linear and nonlinear material models are used for the constitutive relations with thermo-mechanical coupling.

The balance of linear momentum in a solid continuum can be expressed for the current and reference configurations in terms of the Cauchy stress, σ and the first Piola-Kirchhoff stress, $\boldsymbol{P}$, respectively.

$$\begin{aligned} \mathrm{div}\sigma + \rho \mathbf{b}_m &= \rho \dot{\boldsymbol{v}} \\ \mathrm{Div}\boldsymbol{P} + \rho_0 \boldsymbol{b}_m &= \rho_0 \dot{\boldsymbol{v}} \end{aligned} \tag{4}$$

where ρ is the mass density, $\mathbf{b}_m$ is the body force, $\boldsymbol{v}$ is the particle velocity and the 0 subscript denotes a quantity in the reference configuration.

In order to address incompressibility locking, a mixed method which modifies the interpolation of the deformation gradient is used[10]. The modified deformation

gradient is based on a separation of the deformation gradient $\boldsymbol{F}$ into volumetric and deviatoric parts.

$$\boldsymbol{F} = \boldsymbol{F}_{\text{vol}}\boldsymbol{F}_{\text{dev}} \tag{5}$$

In constructing the modified deformation gradient, a mixed treatment replaces the volumetric part. The modified deformation tensor, $\bar{\boldsymbol{F}}$, is defined using a new field variable, θ, for the determinant of the deformation gradient.

The structural formulations (beams and shells) are expressed in resultant form[11-12]. The exponential map is employed for rotational updates which are geometrically exact and singularity free. The structural elements are coupled to general material models using numerical integration of the constitutive relations through the thickness direction.

5. Heat Transfer

The energy balance equation for heat transfer in a solid body has the form

$$\rho c_v \frac{\partial T}{\partial t} = -\text{div}\boldsymbol{q} + r \tag{6}$$

For isotropic heat conduction using Fourier's Law in a solid material with constant properties, this reduces to

$$\frac{\partial T}{\partial t} = k\ \text{div}\,(\textbf{grad}\,T) + r \tag{7}$$

Density, ρ, specific heat, c_v, and thermal conductivity, $\boldsymbol{k}$, are material-dependent variables. The origin of the volumetric heat source, r, differs depending on the type of analysis, e.g., in a thermomechanical problem, the heat source can take the form of either heat dissipation from inelastic deformations of the body, or structural heating from thermal strains and temperature variations in the material properties.

Convective heat flux boundary conditions are applied to element surfaces on a boundary Γ_h. A convective heat flux describes the heat flow from a solid body to a surrounding fluid using Newton's Law of cooling.

6. Multiphysics Interfaces

Interactions between regions are enforced with unstructured mesh *interfaces* (figure 2). This approach is designed to allow variable mesh densities and element topologies at the region interfaces (figure 3).

A slave-master algorithm is used to define the discrete interface constraints of multiphysics problems[9]. These constraints are enforced with the augmented Lagrangian formulation.

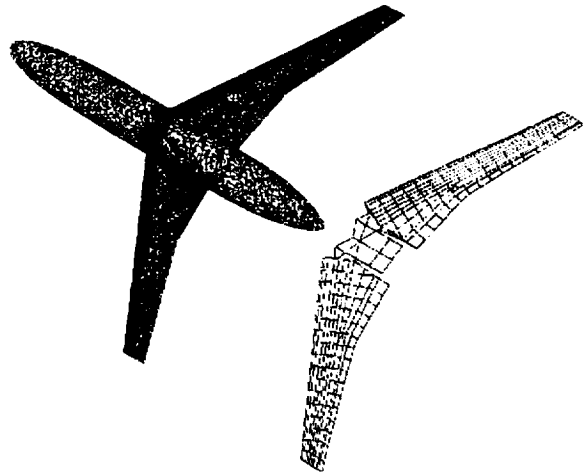

Figure 3. Mesh discretization for the aeroelastic simulation of the ARW2 wing. The fluid and solid surface grids vary in topology and density.

7. Parallel Processing

The same architecture that supports multiple physics simulation naturally and cleanly supports independent and parallel computation. For each problem, we maintain the concept of multiple subdomains. A subdomain is a collection of regions which are uniform with respect to linear solution technology (e.g., iterative, direct, etc.).

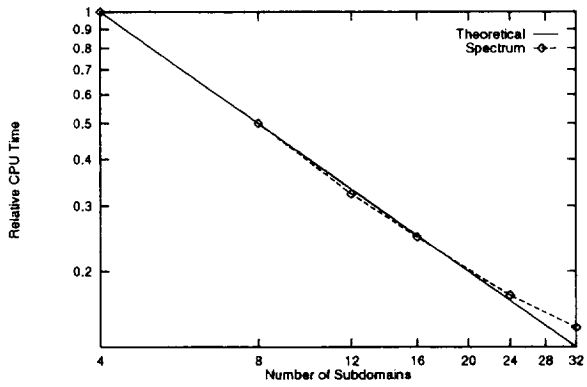

Figure 4. Scalability of a 250K element socket flow. Near-theoretical scaling with superlinearity at 12 and 16 subdomains is observed.

The Same-Program Multiple Data (SPMD) model is implemented via message-processing. In this case, there is support for a wide range of hardware platforms with the standard message-passing interfaces of PVM and MPI. This programming model has the advantage of

allowing the reuse of large portions of code from the uniprocessor version. Excellent performance has been demonstrated on a number of different parallel systems for large, multiphysics simulations (e.g., figure 4). The relative ease of programming and support as well as the portability, scalability and wide availability of systems supporting SPMD make it the preferred model for our applications.

Figure 5. Domain decomposition illustration.

The decomposition of the computational domain (figure 5) is an active area of research which has produced many algorithms and general purpose tools[13-15]. Many decomposition methods commonly use the recursive spectral bisection (RSB) approach[13]. A significant cost of the RSB method is associated with the computation of eigenvectors of a Laplacian matrix constructed from the adjacency structure of the mesh. Hendrickson and Leland introduced a multi-level implementation for the construction of the Laplacian matrix, resulting in significant CPU performance improvement[14]. Karypis and Kumar present a rigorous analysis of multilevel methods and demonstrate analytically their effectiveness[15].

A common feature of most domain decomposition research is the focus on single homogeneous grid applications. In order to support multiphysics simulations, algorithms which extend the multilevel method of Karypis and Kumar to heterogeneous interfaced discretizations are used in the present approach.

To take full advantage of the architecture described above, a multi-subdomain solver is employed to solve the matrix set of equations which result from the discrete finite element problem. In this context, the solver is composed of one global solver and a set of local subdomain solvers. At the subdomain level, the local solver may be explicit, implicit iterative or implicit direct. The local subdomain solver may vary from subdomain to subdomain. The global solver must be implicit iterative.

Two iterative solvers are used for multiphysics problems: the preconditioned conjugate gradient (CG) and generalized minimum residual (GMRES) methods. CG is used for symmetric systems which arise, e.g., from solid linear momentum, heat transfer and mesh movement equations. GMRES is used for non-symmetric systems which arise, e.g., from the fluid linear momentum, thermal, scalar transport, and turbulence equations.

8. Multiphysics Applications

Four applications are presented here to demonstrate the applicability of multiphysics simulation in thermal management and fluid-structure interaction problems.

8.1. Panel Flutter

A 2-D panel flutter problem is used to validate the methods developed in this work and illustrate the difference between linear and nonlinear aeroelastic computations. The problem consists of supersonic flow over a flat plate which is clamped on both ends (figure 6). The panel is initially flat, with a constant freestream pressure on both sides. An analytical solution exists for the linear aeroelasticity problem: with the panel characteristics listed in the table below, the stability limit (i.e, the flow speed above which flutter occurs) for the panel is at Mach 2.

Property	Value	Property	Value
Young's Modulus	77.28 GPa	Length	0.5 m
Poisson's Ratio	0.33	Thickness	1.35 mm
Density	2,710 kg/m^3	Pressure	28 kPa

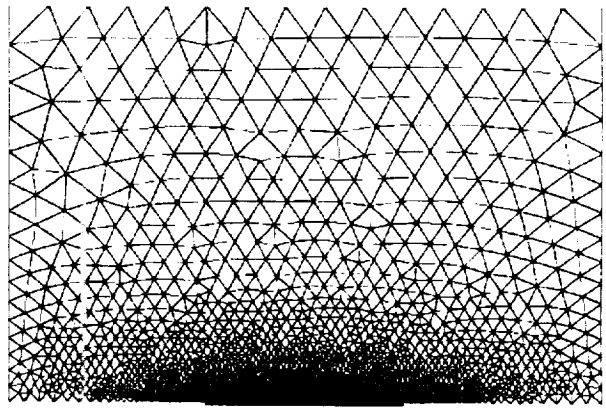

Figure 6. Mesh discretization of the panel flutter problem.

To perturb the instability, the lower side pressure is dropped by 0.1% for 4 milliseconds. Thereafter, the pressure is brought back to 28 kPa. The flow is assumed inviscid (compressible Euler equations). Within each time-step, the FSI equations are solved in a staggered order. The multi-subdomain solver is used for this anal-

ysis. The fluid region is one subdomain with the solid and interface regions combined in a second subdomain. In the fluid subdomain, GMRES is used for the flow equations, and conjugate gradients are used for the mesh movement equations. A direct solver is used on the second subdomain.

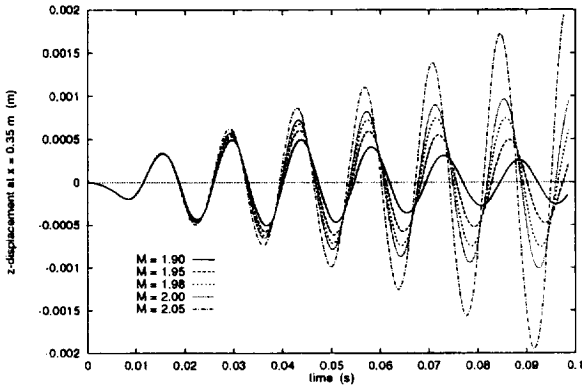

Figure 7. Time histories of the plate deformation at different flow speeds.

Figure 7 plots the time history of the displacement of the panel for several flow speeds using linear elasticity. As seen in the plots, the oscillations of the plate for Mach numbers 1.90 and 1.95 are damped, while the oscillations for Mach numbers 2.00 and 2.05 grow unbounded. The case of Mach 1.98 appears critically damped.

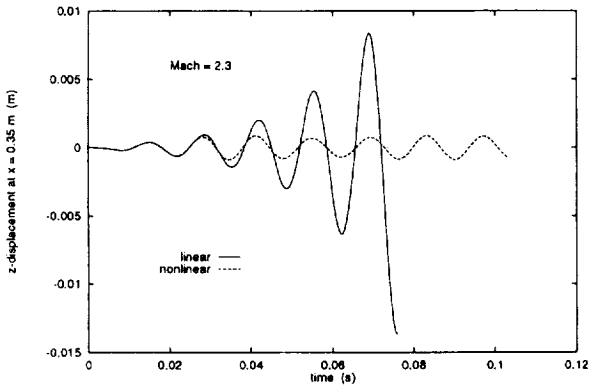

Figure 8. Comparison of the linear and nonlinear aeroelastic response of the panel at M=2.3. Linear theory predicts non-physical exponential growth.

The difference between the linear and nonlinear aeroelastic solutions is depicted in figure 8 for a Mach number of 2.3. The linear solution (consistent with the analytical solution) predicts an unbounded exponential growth of the oscillations of the panel at this unstable speed. The nonlinear solution, however, shows a limit cycle (a result often observed in experiments). The difference between the two solutions can be attributed to the coupling between membrane and bending stresses in the panel with nonlinear elasticity. This phenomenon increases the effective stiffness of the panel with its deformation, which changes the behavior of the system.

Many aerospace components (particularly in military applications) are used beyond the stability limits predicted by the linear theory. The methods developed in this work offer a tool which takes advantage of high-performance computing to predict limit-cycle behavior with nonlinear aeroelasticity.

8.2. AGARD 445.6 Wing Flutter

The AGARD 445.6 standard aeroelastic configuration[16] is used to assess the 3-dimensional application of this method for flutter prediction. The wing is a half-span wind tunnel wall mounted model with a quarter-chord sweep angle of 45 degrees. The configuration has a panel aspect ratio of 1.65 and a tapper ratio of 0.66. The test model is made of mahogany with holes drilled in and filled with foam to add flexibility.

Figure 9. First mode of vibration (9.6 Hz) for the AGARD 445.6 wing.

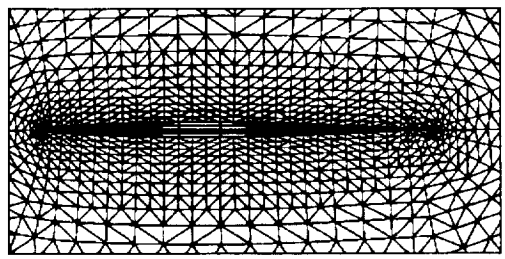

Figure 10. Close-up of the cross-section at the symmetry plane of the fluid-structure mesh.

The first mode of vibration of the wing is depicted in figure 9. A mesh consisting of 118,480 tetrahedral elements and 22,014 nodes is used to discretize the flow domain around the wing. The panel is modeled with 520 hexahedral elements and 770 nodes. A cross-section of the mesh at the symmetry plane is shown in figure 10. The wing is perturbed with a combination of its first two vibration modes applied as initial velocities. No structural damping is used. The oscillations of the structure are then used to compute the damping coefficients. Fig-

ure 11 shows the deformation of the wing (magnified) at two different instances during the oscillation. Also shown are contour lines of the pressure around the wing at several span stations.

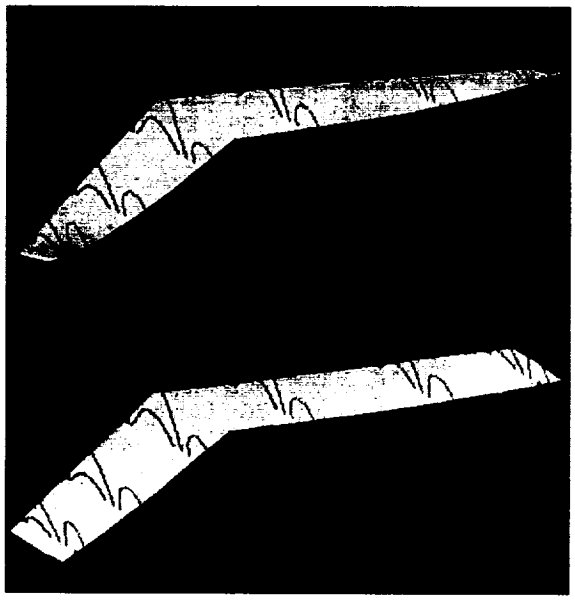

Figure 11. Magnified deformations and pressure contour lines at several stations of the wing. Two frames during the oscillation are shown.

The oscillations of the wing tip are shown in figure 12 for two different values of the dynamic pressure normalized with the experimentally observed flutter value. The figure demonstrates that the predicted oscillations are damped at 90% of the experimental flutter pressure and grow at 110% of that value.

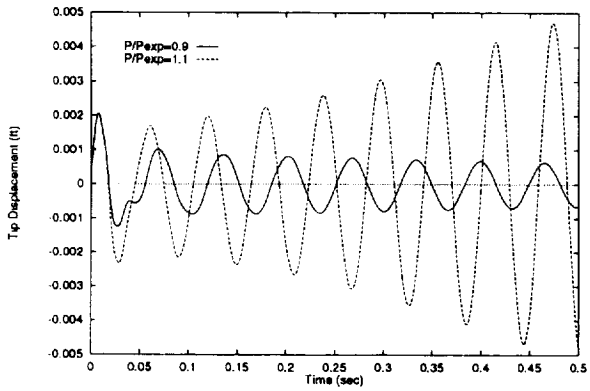

Figure 12. Time history of the tip displacement for the wing at Mach number 0.9 using two values of the dynamic pressure.

8.3. Impeller Flow

The underlying function of turbomachinery equipment, such as pumps, compressors, turbines or fans, is to smoothly impart, or extract, energy from rotating blades to increase, or decrease, the velocity and pressure of a fluid stream. Proper aerodynamic and structural blade design is therefore critical for achieving optimal performance.

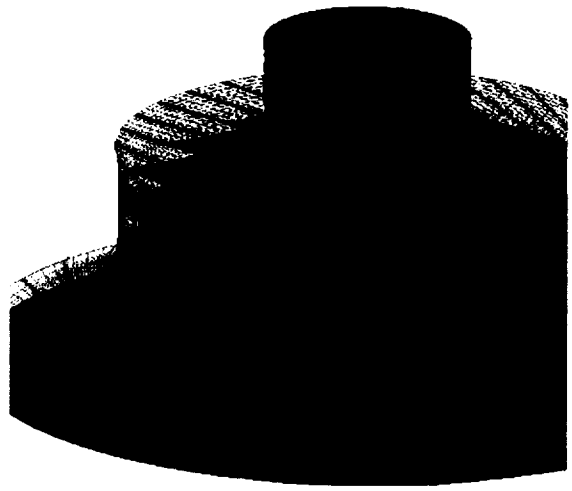

Figure 13. Geometry of the centrifugal impeller study.

The utility of multi-disciplinary analysis and optimization tools for design applications in aircraft propulsion is currently being investigated by the NASA Lewis Research Center. One of the turbomachinery applications involves the simulation of fluid flow through the rotor of an Allied Signal centrifugal compressor. A viscous, steady, compressible flow finite element analysis was performed, in which turbulence was modeled using the Spalart-Allmaras model.

The geometry of the centrifugal impeller analyzed in this study is shown in figure 13. It consists of 17 main and 17 splitter blades located with equal spacing along the circumferential direction. The axial length of the impeller is 3.64 in., whereas its inlet and outer diameters are 2.20 in. and 8.4 in., respectively. The clearance between the main blades and the shroud surface is 0.0033 in. at the leading edge of the blades and 0.0120 in. at the trailing edge of the blades.

The relative frame of reference employed in the current analysis is taken with respect to an observer sitting on the hub and rotating fixed with the wheel around the axial axis of the compressor. In this relative frame of reference, the hub, main and splitter blades are stationary and the shroud is instead rotating in the reverse

direction. This approach greatly simplifies the numerical analysis, because it allows the modeling of the fluid flow passage on a grid that does not change with time, since the shroud has an axisymmetric geometry with respect to the axis of rotation. In addition, due to the cyclic symmetry of the flow, the modeling of only one rotor (main) blade passage is sufficient, which greatly reduces CPU time and memory requirements. For clarification, the notation "cyclic symmetry" in a Cartesian coordinate system corresponds to "periodicity" in a cylindrical coordinate system.

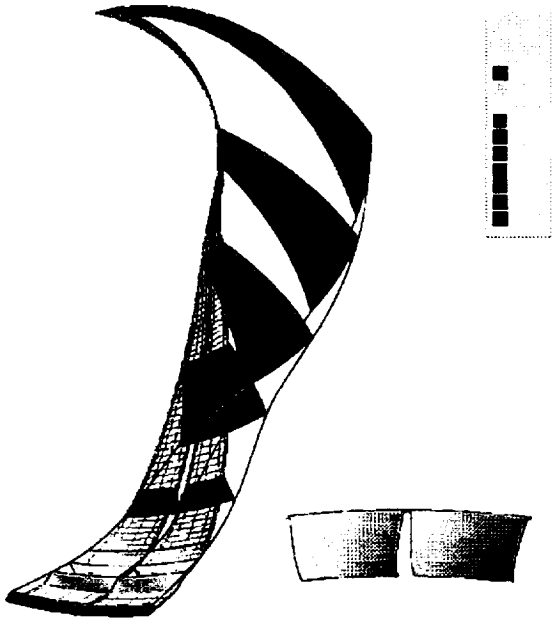

Figure 14. Pressure contours on the flow domain of the centrifugal impeller.

The pressure distribution on several k-surfaces (cross flow surfaces) is shown in figure 14. The pressure rises about 3 atm. in a uniform fashion from the inlet to the exit. As can be seen in the close-up, the pressure is indeed lower on the suction side of the main blade and splitter blade and increases at the pressure side. Further examination revealed small loading on the blade. This is expected, since an off-design condition was considered here. No unloading, however, was found other than at the trailing edge region of the blade.

Contours of the relative Mach number on several blade-to-blade surfaces are shown in figure 15. For the case considered here, the incoming flow at the inlet is at subsonic conditions. The high relative Mach number values seen at the inlet close to the shroud are due to the contribution from the high relative tangential velocity component. The flow appears to become locally transonic at the leading edge of the main blades, which is most likely due to the modeling of the leading edge as a sharp corner rather than as a smooth elliptical surface. Transonic regions are also found near the hub and between the main and splitter blades due to the presence of oblique shock waves. Finally, a recirculation region was found that originated upstream of the leading edge of the main blade close to the shroud.

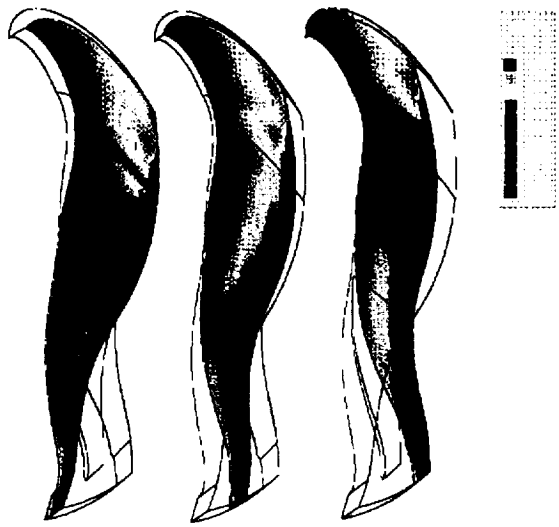

Figure 15. Mach number contours at different stations within the flow domain of the centrifugal impeller.

8.4. Hypersonic Cowl Lip Cooling

The analysis of high aerothermodynamic loading on the leading edges of future hypersonic flight vehicles leads to a clear thermal FSI problem. For example, to prevent material failure on the engine cowl lip caused by aerodynamic heating (including the shock-on-shock interaction) that occurs at hypersonic flight range, active internal cooling of the leading edges is deemed necessary. As a result, this problem class encompasses external hypersonic (compressible) flow with high heating rates near stagnation points, internal coolant (incompressible) flow through the leading edge with heat conduction and convection, and thermal conduction and thermal stresses in the leading edge structure.

Melis et.al.[17] have conducted experiments in the NASA Lewis Hot Gas Facility to evaluate alternate design concepts of internal coolant passage for the cowl lip. A single-physics analysis to compute the material thermal stress, whereby the external aerothermodynamic loading and internal coolant heat transfer were approximated by empirical correlations, has also been performed. Results were found to be encouraging. Nevertheless, a design tool which incorporates direct multiphysics analysis is

still warranted to accurately characterize the leading edge models.

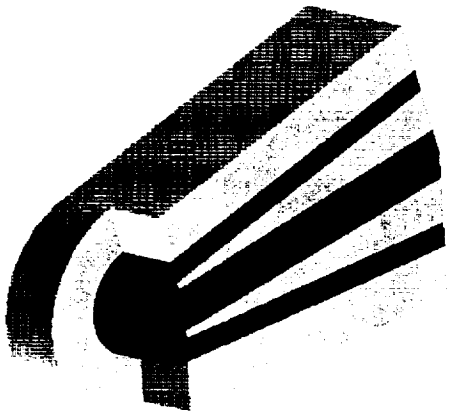

Figure 16. Actively cooled leading edge geometry model.

Work is currently underway to employ Spectrum to perform multiphysics analysis on the impingement-cooled cowl lip model made of nickel. Figure 16 depicts the actively cooled leading edge geometry. The internal coolant (gaseous hydrogen) impinges on the leading edge from the center passage, carries away the heat flux, and returns to the outflow manifold along the lip surface. The coolant is running at high speed but still falls in the incompressible turbulent flow range.

Figure 17. Solid and internal coolant grids for the impingement cooled cowl lip model.

The mesh discretizations for the internal turbulent coolant fluid and the solid component in this fluid-solid interaction problem is shown in Figure 17. Note that the mesh for the internal coolant is highly stretched near the channel walls to account for the sharp gradient in the turbulent boundary layer.

Initial results for the steady-state coolant velocity vector fields and the temperature distribution of the solid are shown in figures 18 and 19. To validate the current analysis, external compressible flow interaction was not considered first. Instead, the external heat loading was simulated by imposing spatial heat flux on the solid surface. It is seen that the flow field has been well resolved, especially the stagnation region on the tip and the corner recirculation region where the flow changes direction are clearly identified. Although turbulence results are not shown, the wall turbulent boundary layer has also been resolved adequately.

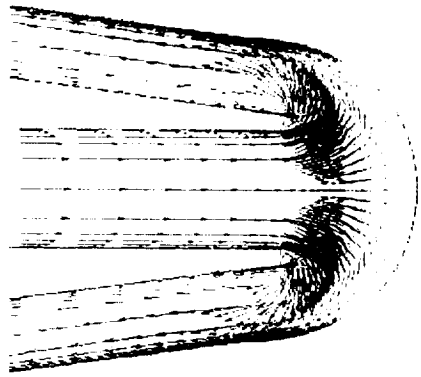

Figure 18. Velocity vectors for the internal gaseous hydrogen flow of the leading edge cooling.

Figure 19. Temperature contours of the solid (nickel) in the leading edge cooling.

In Figure 19, the temperature distribution is found to exhibit a strong gradient in the nose region where the external heat loading is at the maximum. The maximum tip temperature is about 1300 degrees R and levels off to 600 degrees downstream. The inlet coolant temperature is set at 500 degrees and it reaches a maximum temperature of about 750 degrees in the nose region.

8.5. Quenching Process Simulation

A quenching process is relatively rapid cooling of a workpiece by immersion into a fluid after some high-temperature metal-forming operation. It is an integral part of a manufacturing process as it helps determine the materia properties of the finished component created from the workpiece. Quenching is a multi-physics problem: heat transfer from the solid to the fluid induces flow which alters the cooling behavior. Moreover, the overall objective of a *complete* simulation would be to

include the effects of solid deformation and nonlinear material response such as plasticity.

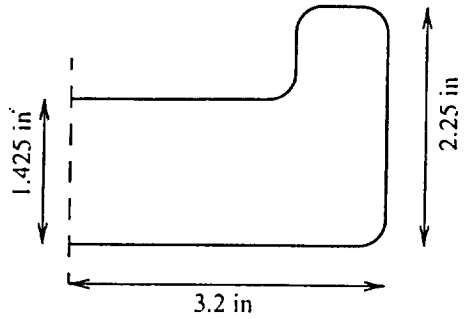

Figure 20. Cross-sectional dimensions of a steel forging (axisymmetric).

For this initial investigation, a thermal-only quench problem for a simple disk was specified. The physical dimensions of the forging are indicated in figure 20. The overall geometry of the quench tank and the location of the immersed forging are illustrated in figure 21. The idealized simulation begins with the disk already in the tank at a temperature of 2000 °F surrounded by fluid at 107 °F. The subsequent five minutes of cooling are assumed to ignore heat transfer into the air from the oil surface. Effects associated with boiling of the quenchant were also neglected.

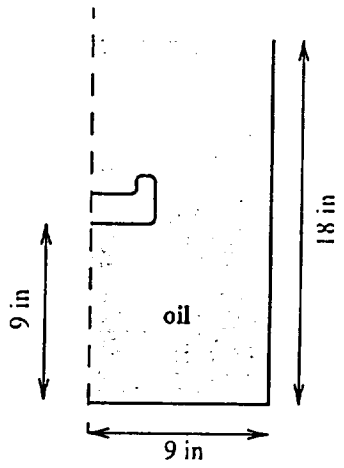

Figure 21. Schematic cross-section of the quench tank.

The quenchant is modeled as an incompressible fluid. The effect of thermal buoyancy is captured by the Boussinesq approximation, which maintains a constant density assumption in the equations of motion while adding an effective body force proportional to the expansivity of the fluid and the local temperature variation from the reference (initial) value. The surfaces of the fluid domain corresponding to the tank walls are designated with no-slip velocity boundary conditions and held at a constant temperature equal to the initial fluid temperature of 107 °F. Free surface effects were not included. Instead, the top surface was considered fixed with the vertical velocity set to zero. This surface was considered adiabatic, so no effects of conduction/convection into the surrounding air are modeled. Temperature dependant properties are used to model the oil and steel materials. Figure 22 presents a close-up of the mesh in the vicinity of the forging.

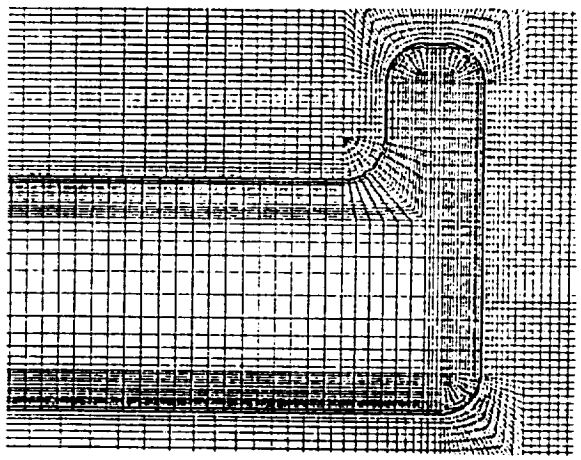

Figure 22. Close up of forging mesh.

In this simulation, automatic time incrementation with a maximum step size of 1.25 seconds was used to model a 300 second forging interval. Figures 23-25 display the system response at time 20.2 seconds. Figure 23 depicts contours of temperature (°F) in the forging and quenchant. Figure 24 shows contours of the magnitude (ft/sec) of the vertical velocity in the quenchant.

The early time response shows a thermal plume developing from the rim of the forging due to heat transfer along the vertical surfaces. This ring-like structure then collapses into a central plume, which is likely to be at least in part an artifact of the axisymmetric assumption of the simulation. Multiple plumes rise from the top horizontal surface and are also subsumed into this central plume. The central plume rises to the surface setting up a recirculation cell in the upper half of the tank.The heated fluid at the bottom horizontal surface of the forging forms a thinner boundary layer of low velocity as the induced buoyancy "traps" the liquid against that surface. It is at this location that neglecting phase change (boiling) of the quenchant is likely most detrimental.

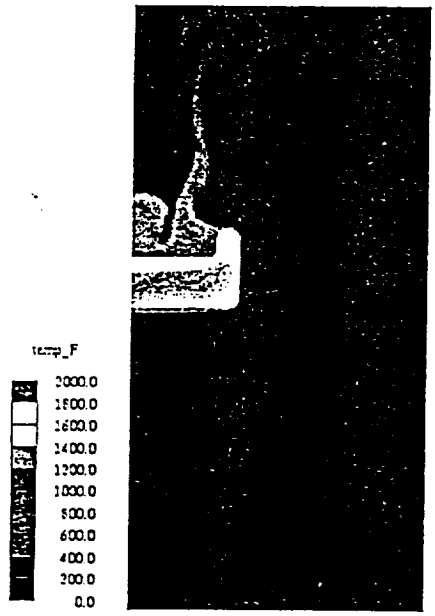

Figure 23. Temperature contours in the forging and quenchant at time 20.2 seconds.

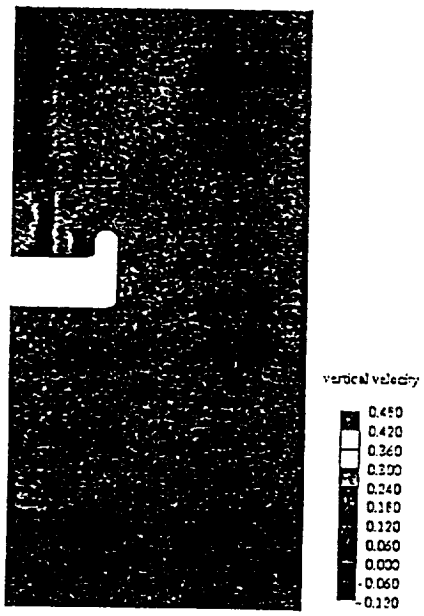

Figure 24. Vertical fluid velocity contours in the quenchant at time 20.2 seconds.

The overall objective of a complete quenching analysis is to determine the thermal history of the forging and hence to subsequently predict the mechanical properties "locked in" the material after the cooling. Figure 25 shows in isolation the thermal contours in the workpiece after 20.2 seconds of quench. The outboard edges of the forging cool most rapidly, as seems intuitive. Perhaps most interesting is some of the local structure exhibited during early time in the temperature contours near the top surface. Here local variations in the quenchant velocities lead to differing cooling rates and local cool spots. Such a mechanism could lead to local variations in material properties which might be a performance issue for the final machined part.

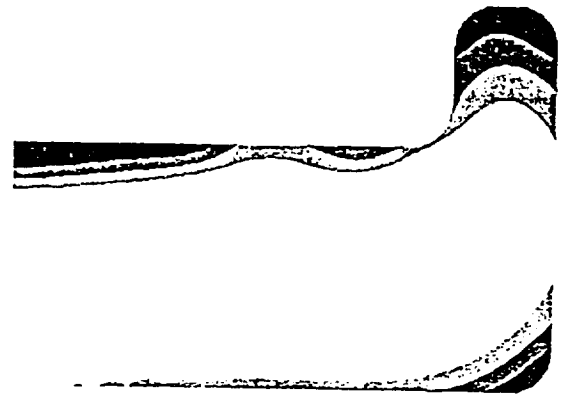

Figure 25. Temperature contours in the forging at time 20.2 seconds.

Conclusions

A multiphysics simulation approach based on the finite element method has been described. This work addresses compressible and incompressible fluid flow, structural, and thermal modeling as well as the interaction between these disciplines. The approach is based on a single computational framework for the modeling of multiple interacting physical phenomena. The augmented-Lagrangian method is used to enforce interaction constraints among all field variables in a fully-coupled manner. Consistent finite element treatments of uniform region balance laws were described within the multiphysics framework. The arbitrary-Lagrangian-Eulerian method is utilized to account for deformable fluid domains.

The efficacy of this method in simulating coupled fluid-solid-thermal interaction was demonstrated with aeroelastic, thermal management and flow-induced vibration problems. The excellent scalability of this approach was illustrated.

Acknowledgment

Portions of this work were supported under the NASA High Performance Computing and Communication Program (HPCCP). Centric gratefully acknowledges this

REPORT DOCUMENTATION PAGE

Form Approved
OMB No. 0704-0188

1. AGENCY USE ONLY (*Leave blank*)	2. REPORT DATE	3. REPORT TYPE AND DATES COVERED
	October 1998	Technical Memorandum

4. TITLE AND SUBTITLE

The Role of Multiphysics Simulation in Multidisciplinary Analysis

5. FUNDING NUMBERS

WU-509-10-31-00

6. AUTHOR(S)

Steven M. Rifai, Robert M. Ferencz, Wen-Ping Wang, Evangelos T. Spyropoulos, Charles Lawrence and Matthew E. Melis

7. PERFORMING ORGANIZATION NAME(S) AND ADDRESS(ES)

National Aeronautics and Space Administration
Lewis Research Center
Cleveland, Ohio 44135-3191

8. PERFORMING ORGANIZATION REPORT NUMBER

E-11373

9. SPONSORING/MONITORING AGENCY NAME(S) AND ADDRESS(ES)

National Aeronautics and Space Administration
Washington, DC 20546-0001

10. SPONSORING/MONITORING AGENCY REPORT NUMBER

NASA TM—1998-208653
AIAA-98-4863

11. SUPPLEMENTARY NOTES

Prepared for the Symposium on Multidisciplinary Analysis and Optimization sponsored by the American Institute of Aeronautics and Astronautics, St. Louis, Missouri, September 2–4, 1998. Steven M. Rifai, Robert M. Ferencz, Wen-Ping Wang, and Evangelos T. Spyropoulos, Centric Engineering Systems, Inc., Sunnyvale, California 94086; Charles Lawrence and Matthew E. Melis, NASA Lewis Research Center. Responsible person, Charles Lawrence, organization code 5910, (216) 433-6048.

12a. DISTRIBUTION/AVAILABILITY STATEMENT

Unclassified - Unlimited
Subject Category: 31 Distribution: Nonstandard

This publication is available from the NASA Center for AeroSpace Information, (301) 621-0390.

12b. DISTRIBUTION CODE

13. ABSTRACT (*Maximum 200 words*)

This article describes the applications of the Spectrum™ Solver in Multidisciplinary Analysis (MDA). Spectrum, a multiphysics simulation software based on the finite element method, addresses compressible and incompressible fluid flow, structural, and thermal modeling as well as the interaction between these disciplines. Multiphysics simulation is based on a single computational framework for the modeling of multiple interacting physical phenomena. Interaction constraints are enforced in a fully-coupled manner using the augmented-Lagrangian method. Within the multiphysics framework, the finite element treatment of fluids is based on Galerkin-Least-Squares (GLS) method with discontinuity capturing operators. The arbitrary-Lagrangian-Eulerian method is utilized to account for deformable fluid domains. The finite element treatment of solids and structures is based on the Hu-Washizu variational principle. The multiphysics architecture lends itself naturally to high-performance parallel computing. Aeroelastic, propulsion, thermal management and manufacturing applications are presented.

14. SUBJECT TERMS	15. NUMBER OF PAGES
Air breathing engines; Simulation; Software tools	17
	16. PRICE CODE: A03

17. SECURITY CLASSIFICATION OF REPORT	18. SECURITY CLASSIFICATION OF THIS PAGE	19. SECURITY CLASSIFICATION OF ABSTRACT	20. LIMITATION OF ABSTRACT
Unclassified	Unclassified	Unclassified	

support as well as that provided by our commercial customers.

References

[1] Eldredge, M., Hughes, T.J.R., Raefsky, R., Ferencz, R., Rifai, S., and Herndon, B., "High-Performance Parallel Computing in Industry," *Parallel Computing*, Special issue on High Performance Computing in Flow Simulations, Eds., Tezduyar, T. and Hughes, T.J.R., Vol. 23, pp. 1217-1233, 1997.

[2] Rifai, Steven M., "Multiphysics Simulation for Coupled Fluids, Thermal and Structural Analysis on High-Performance Computing Platforms," *Proceedings of the 8th Annual Thermal and Fluids Analysis Workshop* (TFAWS 97), NASA Johnson Space Center, Houston, Texas, September 1997.

[3] Hughes, T.J.R., "Recent Progress in the Development and Understanding of SUPG Methods with Special Reference to the Compressible Euler and Navier-Stokes Equations," *Int. J. Num. Meth. Fluids*, Vol. 7, pp.1261-1275, 1987.

[4] Hauke, G. and Hughes, T.J.R., "A Unified Approach to Compressible and Incompressible Flows," *Comp. Meth. App. Mech. and Eng.*, Vol. 113, pp. 3849-396, 1994.

[5] Chalot, F. and Hughes, T.J.R., "A Consistent Equilibrium Chemistry Algorithm for Hypersonic Flows," *Comp. Meth. App. Mech. and Eng.*, Vol. 112, pp. 25-40, 1994.

[6] Jansen, K. Johan, Z. and Hughes, T.J.R., "Implementation of a One-Equation Turbulence Model within a Stabilized Finite Element Formulation of a Symmetric Advective-Diffusive System," *Comp. Meth. App. Mech. and Eng.*, Vol. 105, pp. 405-433, 1993.

[7] Johnson, C, Szepessy, A. and Hansbo, P., "On the Convergence of Shock-Capturing Streamline Diffusion Finite Element Methods for Hyperbolic Conservation Laws," *Mathematics of Computation*, Vol. 54, pp. 107-129, 1990.

[8] Hughes, T.J.R., Liu, W.K., and Zimmerman, T.K., "Lagrangian-Eulerian Finite Element Formulation for Incompressible Viscous Flows," *Comp. Meth. App. Mech. and Eng.*, Vol. 29, pp. 329-349, 1981.

[9] Doghri, I., Muller, A., and Taylor, R.L., "A General Three-Dimensional Contact Procedure for Implicit Finite Element Codes," *Eng Comp.*, to appear.

[10] Simo, J.C., Taylor, R.L., and Pister, K.S., "Variational and Projection Methods for the Volume Constraint in Finite Deformation Elastoplasticity," *Comp. Meth. App. Mech. and Eng.*, Vol. 51, pp. 177-28, 1985.

[11] Simo, J C. and Vu-Quoc, L., "A 3-Dimensional Finite Strain Rod Model. Part II: Computational Aspects," *Comp. Meth. App. Mech. and Eng.*, Vol. 58, pp. 79-116, 1986.

[12] Simo, J.C., Fox, D.D. and Rifai, M.S., "On a Stress Resultant Geometrically Exact Shell Model. Part III: Computational Aspects of the Nonlinear Theory," *Comp. Meth. App. Mech. and Eng.*, Vol. 79, pp. 21-70, 1990.

[13] Simon, H.D., "Partitioning of Unstructured Problems for Parallel Processing," *Comp. Sys. Eng.*, Vol. 2, pp. 135-148, 1991.

[14] Hendrickson, B. and Leland, R., "A Multi-level Algorithm for Partitioning Graphs," Sandia National Labs Rep., Albuquerque, NM 87185-1110.

[15] Karypis, G. and Kumar, V., "Analysis of Multilevel Graph Partitioning," Report 95-037, University of Minnesota, Department of Computer Science, Minneapolis, MN 55455, 1995.

[16] Yates, E.C. Jr., "AGARD Standard Aeroelastic Configuration for Dynamic Response, Candidate Configuration I. - Wing 445.6," NASA TM-100492, 1987.

[17] Melis, M.E., Gladden, H.J., Schubert, J.F., Westfall, L.J. and Trimarchi, P.A., "A Unique Interdisciplinary Research Effort to Support Cowl Lip Technology Development for Hypersonic Applications," NASA Technical Paper 2876, 1989.